Molecular Modeling Study of Dihydrofolate Reductase Inhibitors. Molecular Dynamics Simulations, Quantum Mechanical Calculations, and Experimental Corroboration

Rodrigo D. Tosso,[†,‡] Sebastian A. Andujar,[†,‡] Lucas Gutierrez,[†,‡] Emilio Angelina,[‡,§] Ricaurte Rodríguez,[⊥] Manuel Nogueras,[‖] Héctor Baldoni,[†] Fernando D. Suvire,[†,‡] Justo Cobo,[‖] and Ricardo D. Enriz*,[†,‡]

[†]Departamento de Química, Facultad de Química, Bioquímica y Farmacia, and [‡]IMIBIO-CONICET, Universidad Nacional de San Luis, Chacabuco 917, (5700) San Luis, Argentina

[§]Laboratorio de Estructura Molecular y Propiedades, Área de Química Física, Departamento de Química, Facultad de Ciencias Exactas y Naturales y Agrimensura, Universidad Nacional del Nordeste, Avda. Libertad 5460, (3400) Corrientes, Argentina

[⊥]Departamento de Química, Universidad Nacional de Colombia, Ciudad Universitaria, Carrera 30, No. 45-03. Bogotá, Colombia

[‖]Departamento de Química Inorgánica y Orgánica, Universidad de Jaén, 23071 Jaén, España

S *Supporting Information*

ABSTRACT: A molecular modeling study on dihydrofolate reductase (DHFR) inhibitors was carried out. By combining molecular dynamics simulations with semiempirical (PM6), ab initio, and density functional theory (DFT) calculations, a simple and generally applicable procedure to evaluate the binding energies of DHFR inhibitors interacting with the human enzyme is reported here, providing a clear picture of the binding interactions of these ligands from both structural and energetic viewpoints. A reduced model for the binding pocket was used. This approach allows us to perform more accurate quantum mechanical calculations as well as to obtain a detailed electronic analysis using the quantum theory of atoms in molecules (QTAIM) technique. Thus, molecular aspects of the binding interactions between inhibitors and the DHFR are discussed in detail. A significant correlation between binding energies obtained from DFT calculations and experimental IC_{50} values was obtained, predicting with an acceptable qualitative accuracy the potential inhibitor effect of nonsynthesized compounds. Such correlation was experimentally corroborated synthesizing and testing two new inhibitors reported in this paper.

INTRODUCTION

It is well-known that inhibitors of folate metabolism are quite important drugs in the chemotherapy of bacterial infections and cancer.[1−3] The effectiveness of antifolates is based on the perturbations they cause in the folate pathway, which rapidly lead to nucleotide imbalance and cell death.[2,3] This turns the enzymes involved in this cycle into good targets for chemotherapy. These three enzymes are thymidilate synthase, dihydrofolate reductase (DHFR), and serine hydroxymethyl-transferase. Among them, DHFR have been the main target for the drug design mainly because this enzyme shows important active site differences for different species. DHFR is a key enzyme in the DNA and amino acid metabolism, because tetrahydrofolate is responsible for transporting monocarbon residues for the synthesis of nucleotides and amino acids.[4]

The structural requirements for potential DHFR inhibitors are summarized in recent review articles.[5−8] The availability of high resolution crystal structures of *Pneumocystis carinii* DHFR and human DHFR has provided impetus in the use of rational drug design techniques for the development of highly potent

and specific DHFR inhibitors.[9,10] Thus, DHFR antagonists have been extensively studied and are currently used for the treatment of cancer,[11,12] psoriasis,[13] autoimmune diseases,[14−16] malaria,[17] bacterial and fungal infections, and infections by opportunistic microorganisms associated with AIDS.[18−24] Such inhibitors have been classified according to their structures, classical and nonclassical. The former have a structure similar to folate, where they possess a ring which is generally a pteridine connected to an aryl group and a moiety of glutamate. These antifolates need a carrier called RFC-1 to enter the cell and also undergo a process catalyzed by the folylpolyglutamyl synthetase (FPGS).[25] Within this type of inhibitors are methotrexate (MTX)[26] and pralatrexate (PDX).[27] Nonclassical antifolates lack the tail of glutamate; therefore, are less soluble in water than classical inhibitors, pass through the membrane without using a carrier, and also are not substrates of the enzyme FPGS. Included in this group of inhibitors are trimethoprim (TMP),[28]

pyrimethamine (PYR),[29] trimetrexate (TMQ),[30] and piritrexim (PTX).[31] Recently Goldman et al. reported an interesting review on this topic.[32]

Availability of a large number of high resolution crystal structures of human DHFR provide a solid platform for structure-based design studies for potent and selective DHFR inhibitors.

The challenge is in scoring these poses; an ideal scoring function should be able to reproduce binding energy and should be able to rank the ligands according to their binding affinity. However, the majority of scoring functions, bundled with docking packages, often perform poorly in reproduction of binding affinity; hence, use of these scoring functions is limited to screening of databases of a large number of ligands. In order to predict binding affinity of small molecule inhibitors, a variety of postdocking methods have been established. These methods range from simple consensus scoring to free energy perturbation (FEP).[33−36]

Bag et al.[37] described design, synthesis, and biological evaluation of fourteen structurally diverse compounds. The top five docked poses using Glide-XP[38] score were minimized using the local optimization feature in Prime,[39] and the energies were calculated using the OPLS-AA force field[40] and the GBSA continuum model.[41] Thus, a variety of methods ranging from simple docking scores, to computationally expensive and accurate methods like FEP, have been employed to rank order DHFR inhibitors according to their binding energy, with varying success. However, accurate prediction of binding affinity for DHFR inhibitors still remains a challenge. Very recently Kerrigan et al. reported an interesting review about recent progress in MD simulations of DHFR.[42] Authors conclude that "molecular mechanics calculations can work well to model the initial binding step of an inhibitor or substrate with DHFR. However, DHFR continues to be a challenge for free energy estimation methods and caution is recommended when interpreting these results."

In principle, there seems to be a relatively large amount of impressive information about the structural intricacies of inhibitors interacting with human DHFR. However, reality is somewhat different; there is, in fact, only partial information about this interesting and crucial problem. As it has been previously remarked there are in the literature several studies reporting MD simulations for DHFR interacting with different inhibitors.[43,44] However, in comparison to the many MD simulations performed, there are very few simulations specifically focused in the molecular interactions involved in the formation of the ligand−receptor complexes. This situation is compounded by an almost exclusive use of very simple force fields in automatic searches with molecular mechanics calculations. Thus, interesting details about the molecular interactions intricacies of DHFR interacting with its inhibitors remain unknown.

Our study has two main goals; the first one is to try to get a good correlation between the experimental data (IC$_{50}$ values) and the binding energies obtained by theoretical calculations. The second objective is to obtain a detailed description, at the molecular level, of the most relevant interactions in the binding site of DHFR.

Recently, we reported molecular modeling studies on D2 dopamine receptor using a reduced model for its binding pocket.[45−47] This approach allows to perform more accurate quantum mechanical calculations as well as to obtain a detailed electronic analysis using the quantum theory of atoms in

molecules (QTAIM) technique. Using such procedure, in this paper we have performed a molecular modeling study of DHFR interacting with different inhibitors (**MTX**, compounds **1−13** (Figure 1),[48] **16** (Scheme 1), and **18** (Scheme 2)).
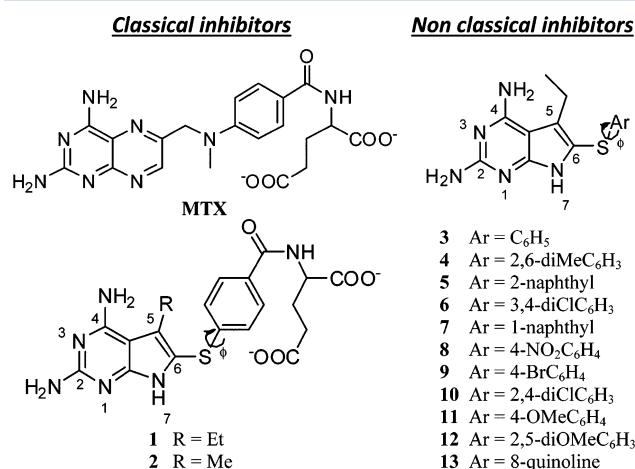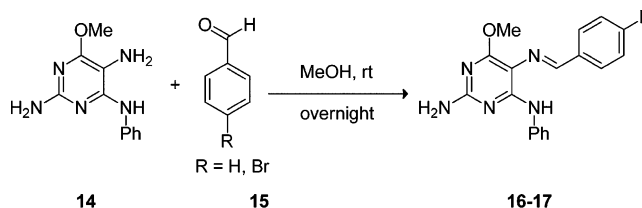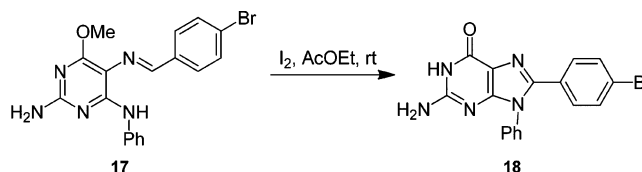

Figure 1. Structures of inhibitors reported by Gangjee et al.[48]

Scheme 1. Synthesis of Imine Derivatives 16−17

Scheme 2. Synthesis of Guanine Derivative 18

■ METHODS OF CALCULATIONS

Our study was carried out in four steps. First, we performed MD simulations of different complexes inhibitor−DHFR. In the second step, MM-GBSA free energy decomposition analysis was employed to choose which residues would be taken into account in our reduced model. Then, each reduced model was optimized using quantum mechanical calculations. Finally, a QTAIM study of these complexes was carried out to acquire structural and electronic knowledge of inhibitor binding to DHFR.

Molecular Dynamics (MD) Simulations. Starting enzyme structure of human DHFR (PDB entry 2W3M) with a resolution of 1.60 Å was obtained from the Protein Data Bank of Brookhaven National Laboratory. The ligand topologies were built using the MKTOP program.[49]

The MD simulations of receptor−ligand complexes were carried out using the GROMACS 4.0 simulation package[50,51] with the OPLS-AA force field[52−57] and the rigid SPC water model[58,59] in a cubic box with periodic boundary conditions. The total number of water molecules was approximately 14 500
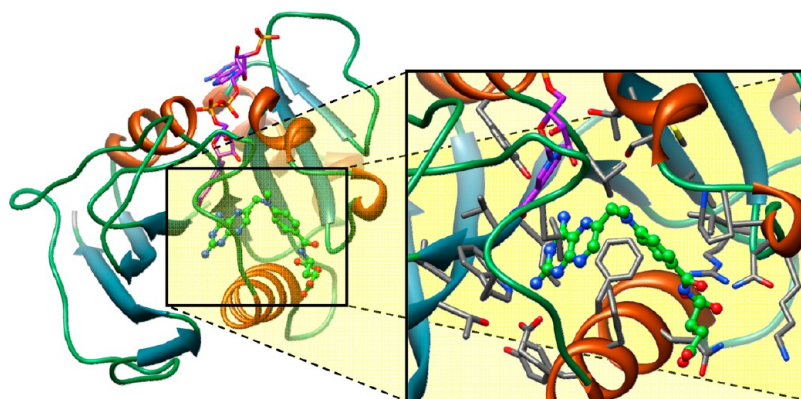
Figure 2. Spatial view of hDHFR with **MTX** (green) and NADPH + H⁺ (purple). Zoom to the active site of the enzyme.

for the different simulations. Five or three Na⁺ ions, depending of ligand charge, were added to the systems by replacing water in random positions, thus making the whole system neutral. Each system was energy-minimized with a steepest-descent algorithm for 1000 steps; then was equilibrated for 100 ps in NVT and NPT ensembles, in order to stabilize the temperature and the pressure of each system, respectively. Finally, a 5 ns MD simulation with a time step of 0.002 ps was performed for each system at 310 K, with constant temperature maintained by the V-rescale algorithm.[60] The compressibility was 4.8×10^{-5} bar⁻¹. Long range interactions were treated by the particle-mesh Ewald (PME)[61,62] method with a 1 nm cutoff and a Fourier spacing of 0.12 nm. All MD analyses were performed using tools available within the GROMACS suite.

The MD simulations in combination with the linear interaction energy (LIE) method were used to calculate ligand–protein binding free energy.[63,64] For such calculations, we use the following equation:

$$\Delta G_{\text{LIE}}^{\text{bind}} = \alpha(\langle V_{\text{l-s}}^{\text{vdW}} \rangle_{\text{bound}} - \langle V_{\text{l-s}}^{\text{vdW}} \rangle_{\text{free}})$$
$$+ \beta(\langle V_{\text{l-s}}^{\text{el}} \rangle_{\text{bound}} - \langle V_{\text{l-s}}^{\text{el}} \rangle_{\text{free}}) \quad (1)$$

where the terms $\langle V_{\text{l-s}}^{\text{vdW}} \rangle$ and $\langle V_{\text{l-s}}^{\text{el}} \rangle$ denote MD energy averages of the nonbonded van der Waals and electrostatic interactions between the ligand and its surrounding environment (subscript l–s), respectively. The α and β parameters are dispersion and electrostatic adjustable energy scale factors,[65] and the values used in these calculations were 0.181 and 0.5, respectively. These values were previously reported by Marelius et al., who adjusted such values for DHFR from experimental parameters.[66]

MM-GBSA Free Energy Decomposition. In order to determine the residues of the active site in DHFR, we first identified the corresponding residues proposed by Oefner et al.[67] and Davies et al.,[68] and then, we employed MM-GBSA free energy decomposition using the *mm_pbsa* program in AMBER12[69] to corroborate which amino acids were interacting with the ligand. This calculation can decompose the interaction energies to each residue considering molecular mechanics and solvation energies.[70–74] Each inhibitor–residue pair includes four energy terms: van der Waals contribution (ΔE_{vdW}), electrostatic contribution (ΔE_{ele}), polar desolvation term (ΔG_{GB}), and nonpolar desolvation term (ΔG_{SA}), which can be summarized as the following equation:

$$\Delta G_{\text{inhibitor-residue}} = \Delta E_{\text{vdW}} + \Delta E_{\text{ele}} + \Delta G_{\text{GB}} + \Delta G_{\text{SA}} \quad (2)$$

For MM-GBSA methodology, snapshots were taken at 10 ps time intervals from the corresponding last 1000 ps MD trajectories, and the explicit water molecules were removed from the snapshots.

Constructing the Reduced Model for the Binding Site. The use of model systems to calculate and simulate molecular interactions (MI) is necessary since the inhibitors interacting at the active site of DHFR constitute a molecular system too large for accurate quantum mechanic molecular orbital (QM MO) calculations and the number of ligands to be screened is large as well. Moreover, a model system representing the DHFR binding pocket may be desirable in order to evaluate the ability of the ligands to interact with the active site. By using a model, complexities due to the rest of the DHFR enzyme are avoided. Thus, a better understanding of the inherent electronic properties of the inhibitors reflected in the MI may be gained. When choosing a model system, the ability to reproduce electronic and hydrophobic properties of the inhibitors is crucial. The questions which arise are the following: how can we select only those amino acids involved in the interactions forming the different E–I complexes? Which might be the best criteria for that? And how can we be sure that all the important interactions have been considered?

To acquire a more detailed insight into the mechanisms driving the bindings of inhibitors to the active site of DHFR, the structure–affinity relationship was analyzed. The information obtained from these calculations is very important for quantitative analyses and is highly useful to the understanding of the binding mechanism. Figures 1S and 2S in the Supporting Information display the spectra obtained for the most representative compounds reported here. A detailed description for the different spectra obtained is also given in the Supporting Information. From these results, we considered it prudent to include in the reduced model, the amino acids involved in the most relevant MI displayed in the different spectra. They are the following: Ile7, Glu30, Phe31, Phe34, Leu67, Arg70, and Val115. In addition, those residues involved in stabilizing and destabilizing interactions displaying more than 1 kcal/mol (Val8, Ala9, Leu22, Trp24, Tyr33, Gln35, Met52, Thr56, Ser59, Ile60, Pro61, Asn64, Lys68, Tyr121, Val135, and Thr136) were also included in the reduced model for the binding pocket of DHFR, and therefore, a final number of 23 amino acids were included in our model. All the water molecules within a 5 Å radius were also included in the reduced model. A spatial view of this model is shown in Figure 2.

Quantum Mechanics (QM) Calculations. Twenty-three amino acids were included in our reduced model. First, the

torsional angles, bond angles, and bond lengths of the flexible side-chains of the amino acids and the ligands of each complex L−R were optimized at the PM6[75] level of theory, using the MOPAC2009 program.[76] On the other hand, the atoms of the backbone were frozen during calculations.

Next, single point calculations of optimized geometries using the Gaussian 03 program,[77] at RHF/6-31G(d) and DFT(PBE/6-31G(d)) levels of theory were performed. For the optimizations of each complex, four different starting geometries from MD simulations were used: the global minimum and three local minima, obtained from the potential energy calculations.

The binding energy (BE) of the complexes was calculated, with the approximation neglecting the superimposition of error due to the difference between the total energies of the complex with the sum of the total energies of the components:

$$BE_{QM} = E_{L/DHFR} - (E_{DHFR} + E_{L}) \tag{3}$$

where BE_{QM} is the binding energy, $E_{L/DHFR}$ is the complex energy, E_{DHFR} is the energy of the reduced receptor model (binding pocket), and E_{L} is the energy of the ligand.[45]

Topological Study of the Electron Charge Density Distribution. Several selected molecular complexes, obtained for our "reduced model system", were used as input for the calculation of the charge density. Single point calculations were realized with Gaussian 03 employing a hybrid PBE functional and 6-31G(d) as basis set.

The topological properties of a scalar field such as $\rho_{(r)}$ are summarized in terms of their critical points, i.e., the points r_c where $\Delta\rho_{(r)} = 0$. Critical points are classified according to their type (ω, σ) by stating their rank, ω, and signature, σ. The rank is equal to the number of nonzero eigenvalues of the Hessian matrix of $\rho_{(r)}$ at r_c, while the signature is the algebraic sum of the signs of the eigenvalues of this matrix. Critical points of $(3, -1)$ and $(3, +1)$ type describe saddle points, while the $(3, -3)$ is a maximum and $(3, +3)$ is a minimum in the field. Among these critical points, the $(3, -1)$ or bond critical points are the most relevant ones since they are found between any two atoms linked by a chemical bond. The determination of all the bond critical points and the corresponding bond paths connecting these point with bonded nuclei were performed with the AIMA11 software.[78] The molecular graphs were drafted using the same program.

It should be noted that QTAIM calculations were carried out using a higher level of computations than that used for geometrical optimization. Thus, from the point of view of the DFT level applied, the PM6-minimized structure is a "random conformation", and some—especially weaker—bonds cannot be correctly identified. Certainly the ideal situation would be to perform structure minimizations at the same computational level than the QTAIM analysis. However, due to the computational cost of performing an energy minimization at the DFT level, it would be necessary to reduce the size of the model system, losing the additive part of the intermolecular interactions (cooperative effects). Therefore, we have preferred to resign some quality and build a reduced model as representative as possible of the active site. The argument is that the QTAIM methodology is relatively insensitive to the method of calculation.[79−81] Therefore, the topological elements which are present at the higher level wave function, though more accurately computed, will be essentially the same than in the lower level wave function, provided that the geometry is the same.

Spatial views shown in Figures 2, 3, and 4 were constructed using the UCSF Chimera program[82] as a graphic interface.
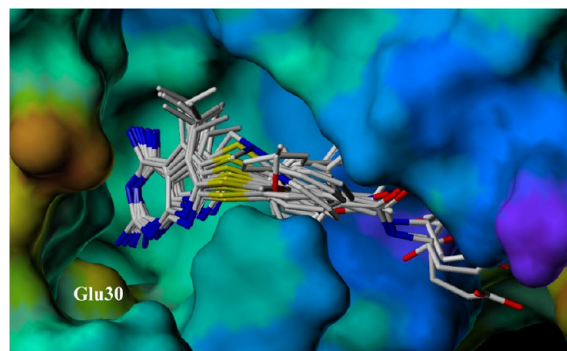

Figure 3. Superimposition of Gangjee's inhibitors in the active site of hDHFR. An electrostatic potential surface of the active site is shown in this figure, where red color denotes regions with negative charge density and blue color denotes regions with positive charge density.
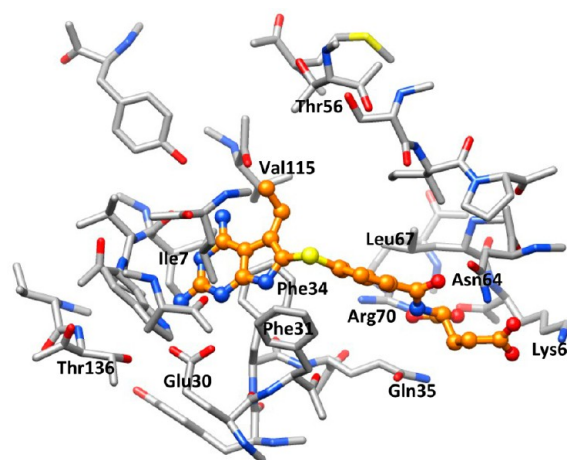

Figure 4. Spatial view of the active site of hDHFR with **IN1**. The names of the residues that give the main interactions are placed. The water molecules were removed for clarity.

■ EXPERIMENTAL SECTION

1. General Experimental Section. *Solvents and Reagents.* Reagents and solvents used were purchased from commercial suppliers and used without further purification procedures.

Chromatography. Thin layer chromatography (TLC) was used to monitor the reaction progress and product purity, it was performed on Merck Kieselgel 60 F254 aluminum precoated plates, and spots were visualized with ultraviolet irradiation.

Melting Points. Melting points were recorded on a Digital Melting Point Apparatus, model IA9300 series, Barnstead Electrothermal, and are uncorrected.

NMR Spectroscopy. One-dimensional (^{1}H, ^{13}C, distortionless enhancement by polarization transfer (DEPT)) and 2D (correlation spectroscopy (COSY), heteronuclear single quantum coherence (HSQC), and heteronuclear multiple bond correlation (HMBC)) NMR spectra were recorded on *Bruker Advance 400* spectrometer. Chemical shifts (δH) are quoted in parts per million (ppm) downfield of tetramethylsilane, and the residual proton of the solvent (δH ((CH3)$_2$SO) =

2.49 ppm) is used as internal reference. Coupling constants (J) are given in Hertz (Hz), and multiplicity abbreviated as follows: d (doublet), t (triplet), dd (double−doublets), m (multiplet). The ^{1}H NMR spectra are reported as follows: δ/ppm (multiplicity, number of protons, coupling constants J/Hz,). DEPT and two-dimensional NMR spectroscopy were used where appropriate to assist the assignment of the signals in the ^{1}H NMR and ^{13}C NMR spectra.

Mass Spectrometry. Low resolution mass spectrometry by electron impact was recorded on a Hewlett-Packard HP Engine-5989 spectrometer (equipped with a direct inlet probe) at *70 eV*. High resolution mass spectra by electron impact were recorded on a *Micromass AutoSpec-Ultima*, magnetic sector mass spectrometer at *70 eV*.

General Procedure for the Synthesis of Imine Derivatives (16−17). In a round bottom flask was added 1 mmol of pyrimidine **14** and 1 mmol of appropriate benzaldehyde **15** in 15 mL of methanol; this solution is stirred overnight at room temperature. The solid formed is filtered off (recrystallized from MeOH if necessary) and dried at 50 °C (see Scheme 1). Data for the compounds **16** and **17** are given below:

6-Methoxy-N^4-phenyl-N^5-[(E)-phenylmethylidene]-pyrimidine-2,4,5-triamine (16). 65% (0.21 g), yellow solid. Mp 151−153 °C. R_f 0.38 (chloroform). IR (ν cm^{-1}): 3336, 3214, 1637, 1560. ^{1}H NMR (DMSO-d_6): δ 3.95 (s, 3H), 6.60 (s, 2H), 7.00 (t, 1H, 8 Hz), 7.29−7.33 (m, 2H), 7.44−7.48 (m, 3H), 7.86 (d, 2H, 8 Hz), 7.95 (d, 2H, 8 Hz), 8.68 (s, 1H), 9.05 (s, 1H). ^{13}C NMR (DMSO-d_6): δ 53.0, 102.6, 120.0, 121.8, 127.6, 128.4, 128.6, 129.8, 137.8, 140.0 153.5, 158.3, 159.7, 161.3. MS (*m/z*, %) (assignation, abundance %): 319 (M$^+$, 43.1), 318 (39.7), 317 (100), 242 (M-Ph, 68.9), 215 (M-104, 68.9), 77 (C$_6$H$_5^+$, 15.2). HRMS calcd for C$_{18}$H$_{17}$N$_5$O: 319.1433. Found: 319.1418.

N^5-[(E)-(4-Bromophenyl)methylidene]-6-methoxy-N^4-phenylpyrimidine-2,4,5-triamine (17). 85% (0.34 g), yellow solid. Mp 184−186 °C. R_f 0.38 (chloroform). IR (ν cm^{-1}): 3359, 3332, 1610, 1562. ^{1}H NMR (DMSO-d_6): δ 3.94 (s, 3H), 6.63 (s, 2H), 7.00 (t, 1H, 8 Hz), 7.31 (t, 2H, 8 Hz), 7.64 (d, 2H, 8 Hz), 7.85 (d, 2H, 8 Hz), 7.92 (d, 2H, 8 Hz), 8.69 (s, 1H), 9.01 (s, 1H). ^{13}C NMR (DMSO-d_6): δ 53.0, 102.5, 120.3, 121.8, 128.3, 128.6, 129.2, 134.1, 136.7, 139.9, 151.7, 158.4, 159.8, 161.4. MS (*m/z*, %) (assignation, abundance %): 397/399 (M/M+2, 26.5:25.6), 396 (9.0), 242 (M—C$_6$H$_4$Br, 100), 215 (M—(N=CH—C$_6$H$_4$Br), 11.1), 77 (C$_6$H$_5^+$, 7.4). HRMS calcd for C$_{18}$H$_{16}$BrN$_5$O: 397.0538. Found: 397.0528.

Procedure for the Synthesis of Guanine Derivative (18). A solution of 1 mmol of imine **17** and 1 mmol of I$_2$ in 20 mL of AcOEt was stirred for 24 h at room temperature. The solid formed is filtered off and washed with a solution of NaHCO$_3$, then with a solution of sodium thiosulfate and, dried in an oven at 100 °C (see Scheme 2). Data for compound **18** are given below:

2-Amino-8-(4-bromophenyl)-9-phenyl-1H-purin-6(9H)-one (18). 72% (0.28 g), beige solid. Mp >300 °C. R_f 0.80 (chloroform/methanol, 9:1). IR (ν cm^{-1}): 3428, 3312, 3155, 1699, 1653. ^{1}H NMR (DMSO-d_6): δ 6.56 (s, 2H), 7.28 (d, 2H, 8 Hz), 7.37 (broad s, 2H), 7.50 (s, 5H, broad band), 7.30−7.60 (m, 5H), 10.71 (s, 1H). ^{13}C NMR (DMSO-d_6): δ 116.5, 122.1, 128.0, 128.8, 129.1, 129.4, 129.8, 131.1, 135.2, 144.0, 153.8, 153.9, 156.7. MS (*m/z*, %) (assignation, abundance %): 381/383 (M/M+2, 100:100), 260 (6), 258 (Ph—N=C—C$_6$H$_4$Br$^+$, 23), 157 (C$_6$H$_5$Br$^+$, 10), 77 (C$_6$H$_5^+$, 35). HRMS calcd for C$_{17}$H$_{12}$BrN$_5$O: 381.0225. Found: 381.0220.

Previous reports indicated that compounds structurally related with molecule **18** displayed an equilibrium between lactam (—HN—C=O) and lactime (—N=C—OH). The preferred form varies in function of the environment (gas phase, aqueous solution, or biological media).[83−85] In order to carry out the molecular simulations, in a previous step, calculations using both forms were performed. Our preliminary study gives similar results for the complexes using lactam and lactime forms. Thus, we chose the lactime form in all the simulations reported here for compound **18**.

Bioassays. The assay is based on the ability of DHFR to catalyze the NADPH-dependent reduction of dihydrofolic acid to tetrahydrofolic acid. The rate of NADPH consumption in the presence of the compound under investigation is monitored by the decrease in absorbance at 340 nm.[86−91] Reactions were performed in a solution containing saturating concentrations of cofactor (80 μM NADPH) and substrate (50 μM dihydrofolate), 50 mM Tris−HCl, 0.001 M 2-mercaptoethanol, and 0.001 M EDTA at pH 7.4 and 30 °C. The enzyme was purchased from Sigma-Aldrich Co. (St. Louis, MO).

■ RESULTS AND DISCUSSION

For this study, structures of inhibitors, whose synthesis and activity had been previously reported by Gangjee et al.,[48] were chosen (compounds **1−13**, Figure 1). We also include in this series **MTX**, a well-known classical inhibitor of DHFR. To corroborate the results, two new molecules (compounds **16** and **18**, Schemes 1 and 2, respectively), possessing significant structural differences to those reported in ref 48, were included in the correlation. In addition, in order to obtain an experimental corroboration, both compounds **16** and **18** were synthesized, and their inhibitory effects on DHFR were tested. The experimental data (IC$_{50}$ values) obtained for these compounds are summarized in Table 1.

MD Simulations. As pointed out in the Methods of Calculations section, the study was carried out in different steps. First, MD calculations were performed simulating the molecular interactions between compounds shown in Figure 1 and the human DHFR enzyme (Figure 2). The X-ray structure

Table 1. Inhibitory Concentrations (IC$_{50}$) against Human DHFR^a

compound	IC$_{50}$ (μM)
MTX	0.022 ± 0.002
1	0.066 ± 0.006
2	0.21 ± 0.021
3	18 ± 1.8
4	32 ± 3.2
5	6 ± 0.6
6	2.8 ± 0.28
7	2.9 ± 0.29
8	5.8 ± 0.58
9	2.7 ± 0.27
10	1.4 ± 0.14
11	2.9 ± 0.29
12	5.8 ± 0.58
13	1.4 ± 0.14
16	68.01 ± 6.8
18	54.45 ± 5.4

^{a}Data of **MTX** and compounds **1−13** were taken from ref 48; whereas IC$_{50}$ values of compounds **16** and **18** are reported in this work.

of the DHFR was minimized before the application of modeling techniques. After 20 ns of simulation, the root-mean-square deviation (RMSD) of the minimized protein structure was 0.176 nm with respect to the starting coordinates. The corresponding RMSD for the backbone and side-chain atoms were 0.111 and 0.216 nm, respectively. Constrains were not used during the minimization.

Comparing the results obtained for the different complexes, interesting general conclusions might be drawn. Consistent with previous experimental[67] and theoretical[42,43] results, our simulations indicate the importance of the negatively charged glutamic acid 30 (Glu30) for the binding of these ligands. A highly conserved Glu30 in αI helix is important for the binding of inhibitors to the human DHFR, and its terminal carboxyl group may function as an anchoring point. In the present study, all the simulated compounds were docked into the receptor with the N_1 and 2-amino group near to Glu30. After 5 ns of MD simulations, the ligands moved slightly but in a different way compared with the initial position. However, the strong interaction with Glu30 was maintained for all the complexes (see Figure 3), supporting the suggestion that Glu30 functions as an anchoring point for this type of ligands. There are many other molecular interactions stabilizing and destabilizing the different complexes, being the following the most significant ones: $\pi\cdots\pi$ stacking interactions with Phe31 and Phe34, and hydrophobic interactions with Ile7 and Val115. In the case of classical inhibitors, they also displayed a bridge salt with Arg70 and hydrogen bonds with Asn64 and hydrophobic interactions with Leu67 stabilizing the flexible side-chain. It should be noted that these results are in agreement with those previously reported from theoretical[42,43] and experimental data.[67,92,93]

Next, the BE obtained for the different complexes were evaluated as relative energies from $\Delta\Delta G$ values. These calculations were performed using eq 1. The energetic components obtained from LIE calculations are given in Table 1S in the Supporting Information. From our MD simulations, a very good binder can be differentiated from a very weak binder (1.26 kcal/mol for compound **1** vs 8.30 kcal/mol for compound **3**), but ligands with similar binding affinities cannot be easily differentiated (6.99 kcal/mol for compound **5** vs 8.34 kcal/mol for compound **7**). This is not an unexpected result; can we realistically expect to make accurate and reliable predictions that are decidedly crude representations of the molecular interactions involved in the binding process? It should be noted that MD simulations neglect or poorly approximate terms that might be playing determinant roles such as lone pair directionality in hydrogen bonds, explicit $\pi\cdots\pi$ stacking polarization effects, hydrogen bonding networks, induced fit, and conformational entropy. Thus, we cannot expect to obtain clear differences between compounds possessing relatively similar binding energies. At this stage of our work, we consider the trend predicted for the MD simulations as certainly significant. However, they might be reluctant to give a quantitative significance because of the approximations involved in this mode of approach. It should be noted that we are dealing with relatively weak interactions and therefore MD simulations might underestimate such interactions.

Thus, in the next step of our study, reduced model systems were optimized using combined semiempirical, ab initio, and DFT calculations.

Quantum Mechanics Calculations. PM6 optimizations were performed considering all receptor amino acids that might

interact after initial positioning of the ligands against Glu30 residue. Next, RHF/6-31G(d) and DFT (PBE/6-31G(d)) single point calculations were carried out for each complex optimized from PM6 computations. Figure 4 shows the complex obtained for inhibitor **1** optimized at PM6 level of calculations.

Once the BE values of the different complexes were obtained from the theoretical calculations, the different correlations between the theoretical calculations and the experimental data (IC_{50}) reported in ref 48 were calculated.

Considering only **MTX** and compounds **1−13**, the following correlation coefficients R^2 = 0.78, 0.77, and 0.77 were obtained, using PM6, RHF/6-31G(d), and PBE/6-31G(d) calculations, respectively. These results are very satisfactory, considering the type of approximation used. From these results, it appears that the predicted first-principles structure of the primary binding pocket of DHFR leads to correct predictions of the critical residues for binding inhibitors and gives relative binding affinities that correlate fairly well with those obtained in experiments.[48]

PM6, ab initio, and DFT calculations performed here may not properly consider the dispersion interactions. Fortunately, in this case, it appears that such limitations are not severe enough to prevent us from obtaining our goals. Such an assumption appears to be reasonable, considering the significant correlation obtained between the experimental data and the theoretical calculations performed. However, a kind of error-cancelation might have taken place, in which case the approaches used in this study might be operative only for the classical and non classical inhibitors reported by Gangjee et al. An additional validation and more calculations might be required to extend these approaches to other compounds possessing different structures.

Theoretical and Experimental Corroboration for the Correlation Obtained from QM Calculations. Two new compounds keeping some structural resemblance with the molecules reported by Gangjee et al. but at the same time possessing significant structural differences were included in this series in order to know if the correlations obtained from QM calculations using a reduced model system are good enough to predict the activity of compounds possessing structural differences. The compounds selected to test our theoretical results were compounds **16** and **18** (see Schemes 1 and 2). Observing both structures it is clear that some structural resemblance with the compounds reported by Gangjee et al. in the Pyr moiety were maintained although two important changes were introduced. The first one is the replacement of −NH_2 group in Pyr ring by −OCH_3 and −OH in compounds **16** and **18**, respectively. The other important change is the presence of two bulky aromatic rings instead of one; the first ring joined to C6 and the second one joined to N7. This is a significant structural difference with respect to the previously analyzed compounds.

MD simulations for compounds **16** and **18** interacting with DHFR were performed. Figure 3S shows the inhibitor−residue interaction spectra calculated by the free energy decomposition of compounds **16** and **18**. It is interesting to note that both spectra are closely related to those previously obtained for the nonclassical inhibitors (compare Figures 1S, 2S, and 3S), indicating that these new compounds might be inhibitors of DHFR. Note that the only significant difference with the spectra obtained for the nonclassical inhibitors is that the stabilizing interaction of Val115 is very weak for compounds **16**
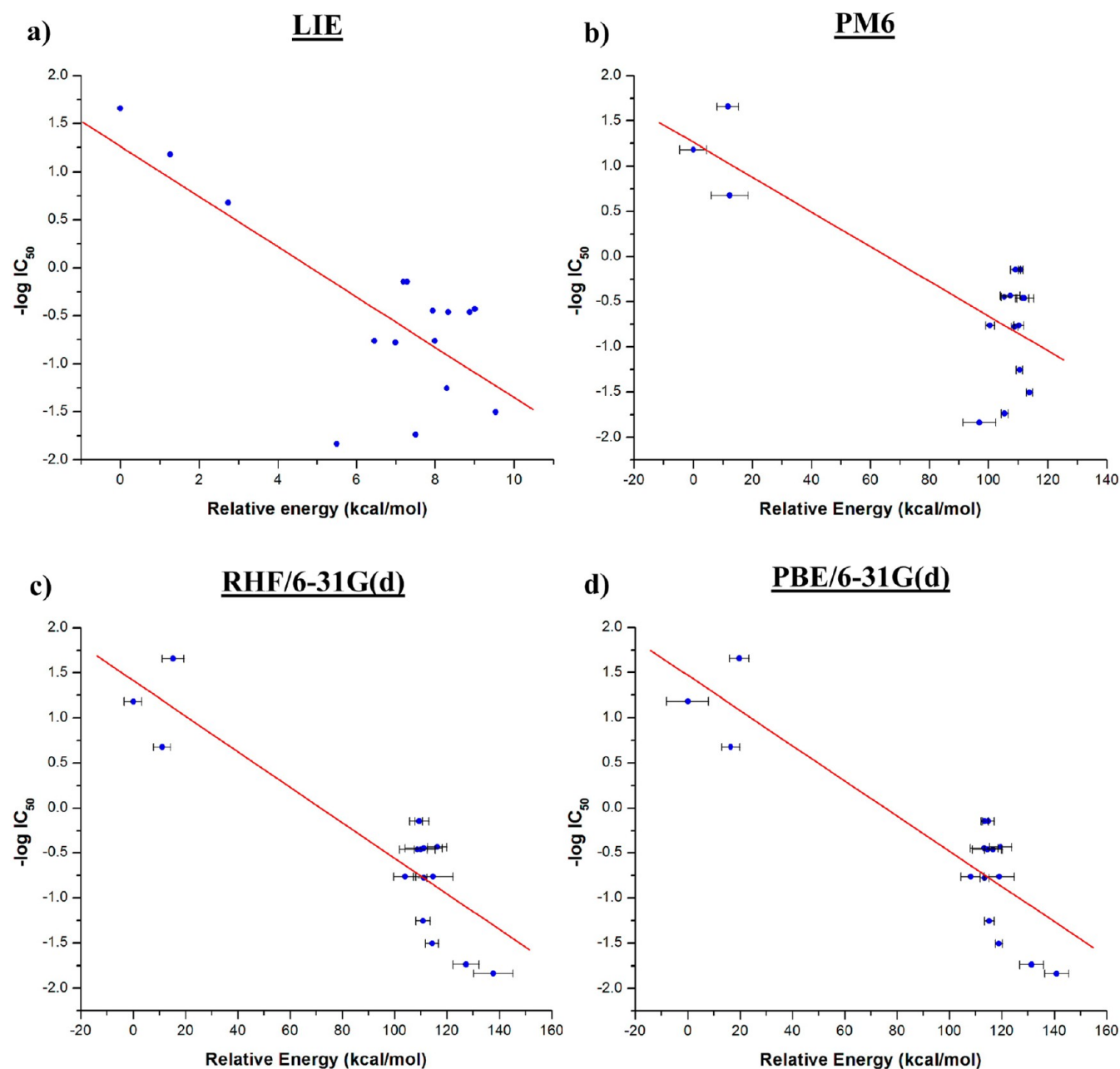
Figure 5. Correlations obtained with different calculation methods. The *x*-axis denotes the binding energy, and the *y*-axis denotes the inhibitory activity value of each compound ($-\log IC_{50}$). (a) Relative energies ($\Delta\Delta G$) from LIE calculations. (b) PM6 relative energies. (c) ab initio (RHF/6-31G(d)) relative energies. (d) DFT(PBE/6-31G(d)) relative energies. The error bars are showing the energy gaps obtained using the different starting geometries from MD simulations.

and **18** in comparison to that observed in the spectra of compounds **3–13**. On the other hand, the binding energy calculated using the LIE approach predicts $\Delta\Delta G$ values of 7.50 and 5.50 kcal/mol for compounds **16** and **18**, respectively. These results predict that compounds **16** and **18** might be at least weak inhibitors of DHFR. In the next step, QM (PM6, ab initio, and DFT) calculations were performed using the reduced model in order to evaluate the BE of compounds **16** and **18**. These results are closely related to those obtained from MD simulations.

Our theoretical results indicated that compounds **16** and **18** might possess an inhibitory effect against the DHFR enzyme. Although the theoretical results predicted a weaker activity for these compounds in comparison to those reported for the

classical and nonclassical inhibitors studied here, we still considered very interesting to synthesize and test the inhibitory activity of compounds **16** and **18** in order to corroborate our theoretical results.

The synthesis of compounds **16** and **18** was performed as described in the Experimental Section. Once compounds **16** and **18** were obtained, their inhibitory effect against human DHFR was evaluated. In order to minimize the experimental errors due to the methodology employed, a very similar experimental protocol to that reported in ref 48 was used (see Experimental Section). Our experimental measurements indicated that compounds **16** and **18** possess IC_{50} values of 68.01 and 54.45 μM, respectively. Both compounds displayed a moderate inhibitory effect, which is in a complete agreement

with our theoretical predictions. These experimental results are an additional support to our reduced model as well as to the correlations obtained from QM (PM6, ab initio, and DFT) calculations. Considering the different structural features of compounds **16** and **18** with respect to the rest of the compounds in this series, the theoretical approaches used and the possible different experimental conditions in the Bioassays, these results are very encouraging. It should be noted that our theoretical calculations predicted BE for compounds **16** and **18** comparable to those of the nonclassical inhibitors, which is in complete agreement with the experimental IC_{50} values obtained here.

With the theoretical (BE values) and experimental (IC_{50} values) data for compounds **16** and **18**, the correlations obtained from LIE, PM6, ab initio, and DFT calculations were recalculated for the whole series. Figure 5a shows a graphical representation of the calculated BE obtained from LIE calculations versus the experimental $-\log IC_{50}$ values. This figure has a correlation coefficient $R^2 = 0.58$. Figures 5b, c, and d show the same correlation but in this case using BE obtained from PM6, RHF/6-31G(d), and DFT(PBE/6-31G(d)) calculations, respectively. Such drafts displayed the following correlation coefficients R^2: 0.64, 0.78, and 0.78, indicating that ab initio and DFT calculations give a better correlation with the experimental data. Although the three linear correlations obtained are good enough to predict the biological activity of these inhibitors, it is evident that ab initio and DFT calculations give a better correlation with respect to the semiempirical computations. It should be noted that the trend line for the models is in fact connecting two clusters of data. It is clear that within each cluster, the correlation would be worse. However, the obtained models are quite good in placing the studied compounds into one of two groups, "very good binders" (the classical inhibitors which are the most active compounds in this series) and "weak binders" (the set of nonclassical inhibitors and less active compounds). It is evident that such information is valuable and successful. From our results it is clear that these approaches allow obtaining correct predictions even including compounds structurally different in the calculations and provide relative binding affinities that correlate fairly well with that obtained from experiments. Although there are numerical differences between the experimental and theoretical values obtained, it is evident that both correlations (ab initio and DFT) are still good enough to predict the inhibitory effect for a nonsynthesized compound with an acceptable qualitative accuracy. A particularly interesting characteristic of these correlations is their capacity to predict the inhibitor effect of compounds possessing significant structural differences (compare compounds **16** and **18** with the rest of the series). This is a very important aspect because these correlations could be very useful to test compounds possessing different structural profiles with those of the classical inhibitors.

Trying to take advantage of the reduced models in the second stage of our study, a quantum theory atoms in molecules (QTAIM)[94,95] analysis was carried out. Such accurate calculations are needed to obtain a more detailed description of the molecular interactions that are stabilizing and destabilizing the different complexes.

Evaluating the Molecular Interactions for the Different Complexes Using QTAIM Calculations. The topological analysis of the electron density constitutes a powerful tool to investigate the electronic properties of the molecular

system and allows a deep examination of the molecular interactions. This methodology has been successfully applied in the study of the properties of a variety of conventional and unconventional hydrogen bonds (HBs), aromatic HBs as well as $\pi\cdots\pi$ stacking interactions.[96−98] From QTAIM calculations, it is possible to determine in an unequivocal way the different strong and weak interactions between two atoms observing the existence of bond critical points (BCPs) and their respective bond paths. It should be noted that this detailed analysis is not possible only from the evaluation of the geometrical parameters (bond distances and angles). The intermolecular interactions of all the classical and nonclassical antifolates reported here were evaluated using the QTAIM techniques. In order to keep the size of this section, only the most representative results are discussed here. The rest of them might be observed as supplementary data or might be provided by the authors.

Figure 6 shows the main interactions of **IN1** (representative compound of classical inhibitors) at the binding pocket. There
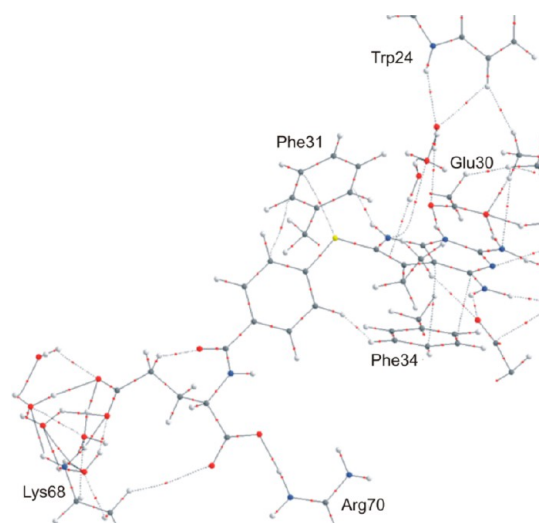

Figure 6. Molecular graph obtained for **IN1** interacting at the binding site.

are three salt bridges formed among the three charged groups of **IN1** (one positive and two negative) with residues Glu30, Lys68, and Arg70, respectively. The hydrogen atoms joined to the N_1 and 2-amino group of 2,4-diamino-5-ethyl-pyrrolo[2,3-*d*]pyrimidine (from now on called **Pyr**) form strong bifurcated H-bonds with the carboxylate group of Glu30. On the other side of the binding pocket, the carboxylate groups located in the C6 flexible side-chain form hydrogen bonds with the positive charged residues Lys68 and Arg70. It is clear that the molecular size of this inhibitor is too large, and therefore, it is very difficult to visualize in detail the different interactions stabilizing and destabilizing this complex using only one draft. Thus, to better appreciate the different MI, such interactions were displayed using two figures: Figure 7a showing the MI of the Pyr ring and Figure 7b showing the MI obtained for the flexible side-chain joined to C6.

Figure 7a shows that the Pyr ring is stacked with the aromatic ring of Phe34. This molecular graph displays the number of BCPs and the corresponding bond paths connecting the Pyr ring atoms of **IN1** with the phenyl atoms of Phe34. There are two BCPs and the corresponding bond paths between Pyr and the phenyl ring of Phe34 (indicated by green arrows). The **DHFR-IN1** complex presents one of the strongest $\pi\cdots\pi$
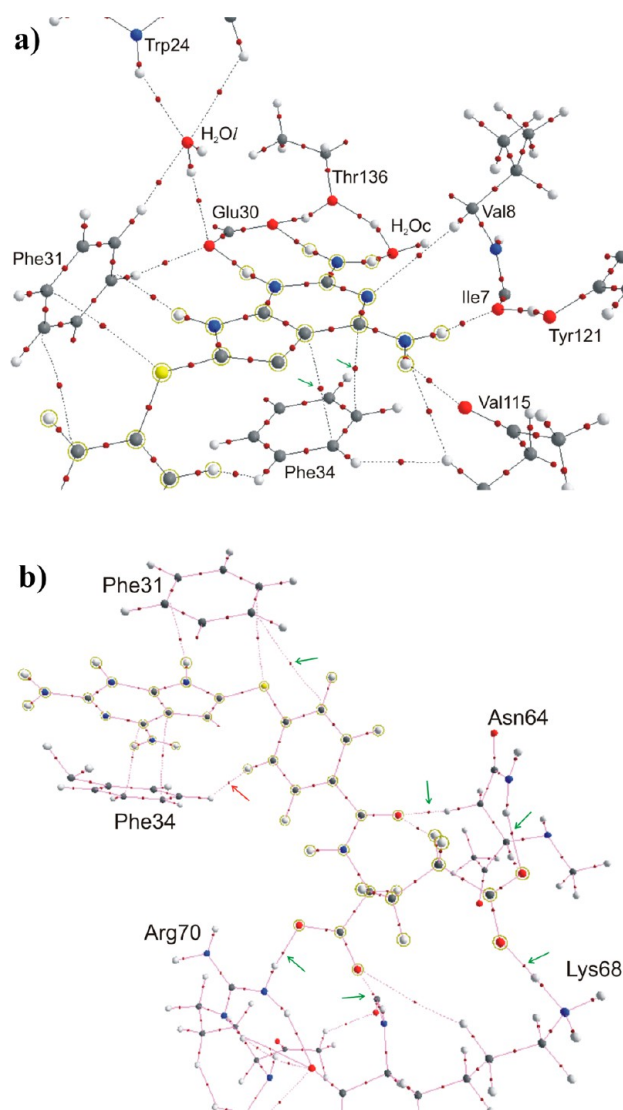
Figure 7. Molecular graphs obtained for Pyr ring (a) and C6-side-chain (b) of **IN1** interacting at the binding site. The net of interactions involving different regions of **IN1** can be observed in this figure. The inhibitor C5-ethyl group has been removed for clarity.

stacking interactions observed in this series between the Pyr ring and Phe34.

It should be noted that the hydrogen atoms at N_1 and 2-amino group of **IN1** form strong bifurcated H-bonds with the carboxylate group of Glu30 (see Figure 1 for atom numbering). Furthermore, the other hydrogen atom located at the 2-amino group forms a strong H-bond with a conserved water molecule. This interaction is present in most of the complexes reported here. This conserved water molecule is indicated as H_2Oc in the molecular graph. Different interactions are observed in relation to the interactions of the 4-amino group of Pyr ring. The two H-atoms of the 4-amino group form bifurcated H-bonds with the oxygen atoms located in the backbone of Ile7 and Val115 residues. These H-bonds might be well appreciated in the molecular graph shown in Figure 7a. Very similar MI were observed for the rest of classical inhibitors reported here (**MTX** and **IN2**).

The interactions between the C6-side-chain and the different residues can be seen as a force pulling the inhibitor toward one side (the positive charged side where Arg70 and Lys68 are located), whereas the interactions between the Pyr ring with Glu30, Ile7, Tyr121, and Val115 (among other residues) pull the inhibitor toward the opposite side of the binding pocket (the negatively charged side of the binding pocket where Glu30 is located). The most relevant interactions of the C6-side-chain moiety of **IN1** with the DHFR binding pocket are indicated by arrows in Figure 7b.

A CO_2^- group from the C6-side-chain forms a strong H-bond with an N—H bond of Arg70; while the other CO_2^- group forms an H-bond with Lys68. Stabilizing C—H···π interactions between C—H bond of the benzene ring and the π-electron cloud of Phe34 are not observed. In fact, just a short C—H···H—C contact is verified between them (indicated by a red arrow).

Next, the MI obtained for **IN3** as the characteristic MI stabilizing complexes of nonclassical inhibitors are reported. In contrast to the classical inhibitors, the nonclassical ones do not present a flexible side-chain possessing carboxyl groups (see Figure 1). Therefore, it is logical to expect different MI in such portions. Figure 4Sa and b in the Supporting Information shows the electron density molecular graphs obtained for the Pyr moiety and the C6 side-chain of compound **3** anchored into the binding pocket.

As expected, the MI observed in the Pyr ring moiety of the nonclassical inhibitors are closely related to those obtained for the same portion of the classical inhibitors. However, some slightly but interesting differences might be appreciated. All the strong stabilizing hydrogen bonds were observed in this complex, but it should be noted that the spatial ordering adopted by the C6 benzene ring is different from that observed in the classical inhibitors. In this case, this ring is partially inserted between the Pyr and phenyl ring of Phe34. This insertion is evidenced by the formation of a C—H···π H-bond between the C6-side-chain benzene ring (H-donor) and the Phe34 π-electron cloud (H-acceptor, see Supporting Information Figure 4Sb). This "insertion" of the benzene ring between the inhibitor fused rings and Phe34 disrupts the possible π···π stacking interactions between both rings.

Supporting Information Figure 4Sb shows that the benzene ring of compound **3** is anchored in the binding pocket by few interactions (indicated by arrows). Consequently, the forces exerted by the interactions of the Pyr ring at the opposite side of the binding pocket are not well counterbalanced, and therefore, this nonclassical inhibitor is displaced toward the negative zone of the binding pocket where Glu30 is located. These results account for the general behavior of the nonclassical inhibitors reported here. A detailed description for the MI observed for the **DHFR-IN5** complex is given in the Supporting Information (Figure 5Sa and b).

In order to compare the binding mode of the classical and nonclassical inhibitors reported by Gangjee et al. with that observed for the compounds here synthesized (compounds **16** and **18**), a virtual horizontal plane formed by the carboxylate group of Glu30 and the oxygen atoms of the carbonyl group located at the backbone of Ile7 and Val115 was defined. In **MTX** and **1**−**13** inhibitors, the Pyr ring systems are anchored within the plane formed by these atoms, allowing N_1—H and 2-amino groups to establish strong H-bonds with Glu30 whereas the 4-amino group might interact strongly with Val115 or Tyr121. In contrast, the equivalent Pyr ring system of compound **18** is anchored below this virtual plane (see Figure 8a). The main consequence of this shifting of the Pyr ring system toward a lower part of the binding pocket is a noticeable
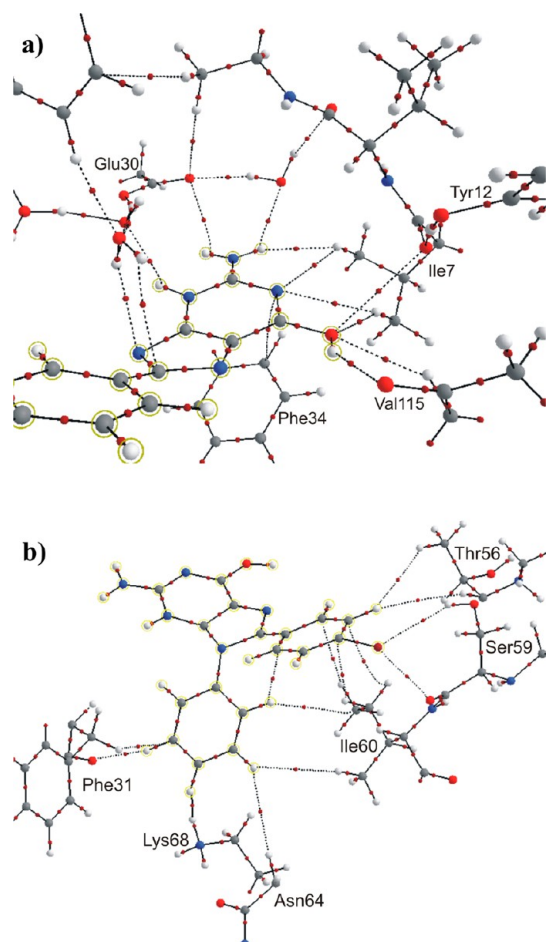
2026

dx.doi.org/10.1021/ci400178h | *J. Chem. Inf. Model.* 2013, 53, 2018−2032

Figure 8. Molecular graphs obtained for equivalent Pyr ring (a) and C6 and N7-side-chains (b) of **IN18** interacting at the binding site. The net of interactions involving different regions of **IN18** can be observed in this figure.

weakening of the interactions between this inhibitor and Glu30. One of the possible factors determining the different binding mode of **18** in the pocket in comparison to the rest of the inhibitors is the replacement of the hydrogen atom of the N_7—H bond by a phenyl group which might cause some steric clash with the Phe31 residue. Another factor determining the anchoring of the inhibitor fused ring system at the bottom of the active site is the different interaction pattern observed for the 4-hydroxyl group in comparison to that displayed by the 4-amino group of the rest of the inhibitors. Since the 4-amino group in Gangjee's inhibitors possesses a double H-donor capacity, the group is H-bonded to both Val115 and Ile7 (or to Tyr121 in some inhibitors). In contrast, the 4-hydroxyl group of inhibitor **18** has a single H-donor capacity, and hence, it acts only as an H-donor against Val115 (BCP, $\rho(r_b)$ = 0.0187 au). It should be noted that the 4-hydroxyl group is also able to form H-bonds through its oxygen lone pairs, and therefore, it is H-bonded to two C—H bonds from Ile7 (BCP, $\rho(r_b)$ = 0.0104 au) and Val115 (BCP, $\rho(r_b)$ = 0.0105 au). These C—H bonds are located below the virtual horizontal plane and the equivalent Pyr system of inhibitor **18** is anchored under such plane. From Figure 8a, it might be appreciated that the N_1—H group of compound **18** is not H-bonded to the carboxylate group of Glu30, whereas the 2-amino group is associated with Glu30 by a rather weak (Glu30)$CO_2^-\cdots H_2N$(2-amino) H-bond ($\rho(r_b)$ = 0.0087 au) in comparison with the same H-bond formed by

Gangjee's inhibitors (displaying $\rho(r_b)$ values from 0.0360 to 0.0600 au). Finally, a weak interaction connecting the 4-hydroxyl oxygen atom with Ile7 oxygen atom ($\rho(r_b)$ = 0.0040 au) is also observed. Thus, the binding mode of inhibitor **18** is clearly weaker in comparison to those observed for Gangjee's inhibitors. On the other hand, as the ring system is anchored at the bottom of the binding pocket, it is quite close to the Phe34 phenyl ring. Due to this proximity, a $\pi\cdots\pi$ stacking interaction is verified between the N3 atom from the ring system and a phenyl carbon atom of Phe34.

As can be seen in Figure 8b, the C6-ring is slightly bent above the plane of the equivalent Pyr ring system due to the C—H$\cdots\pi$ H-bonds formed with the Ile60 side-chain. On the other hand, the N7-ring is somewhat bent below the plane of the fused ring system due to the H-bonds formed with the Phe31 backbone atoms and a strong C—H$\cdots$H—N$^+$ dihydrogen bond formed with Lys68 ($\rho(r_b)$ = 0.0310 au).

It is interesting to note that in compound **16**, the equivalent Pyr system is formed just by one ring (see Scheme 1). Such ring is not stacked over the Phe34 phenyl ring but it is displaced toward the positive charged side of the binding pocket. As can be seen in Figure 9, there are no topological elements that connect the equivalent Pyr ring to the carbon
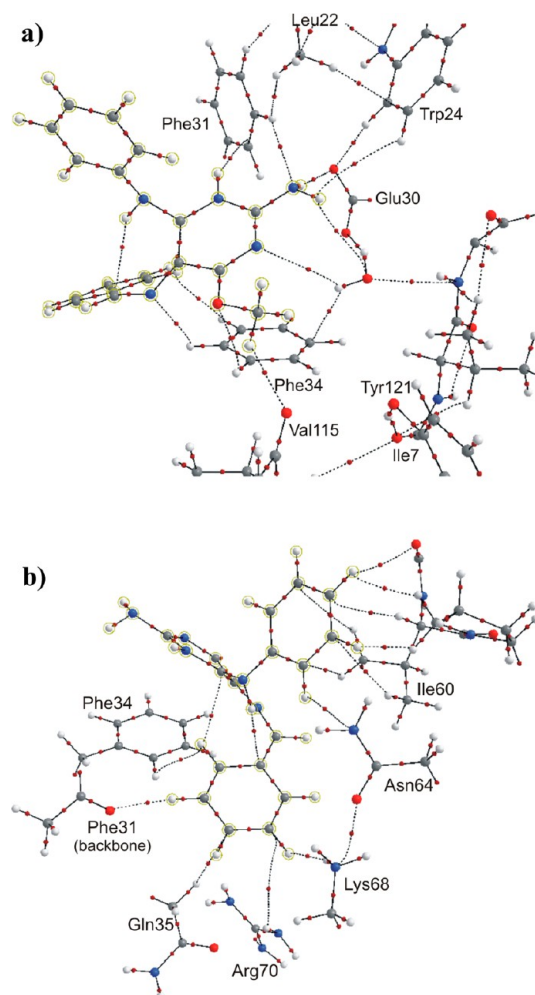

Figure 9. Molecular graphs obtained for equivalent Pyr ring (a) and C6 and N7-side-chains (b) of **IN16** interacting at the binding site. The net of interactions involving different regions of **IN16** can be observed in this figure.
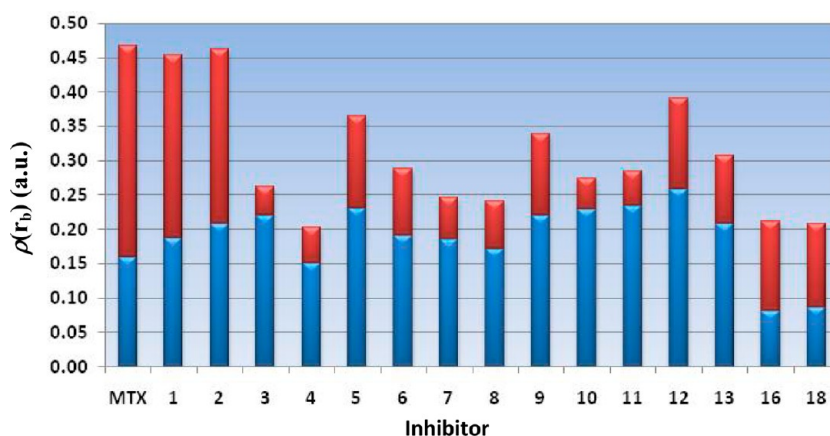
Figure 10. Charge density values for the total interactions of the Pyr ring system (blue stacked bars) and the N7 and/or C6-side-chains (red stacked bars) for the inhibitors at the binding pocket. The repulsive short C—H···H—C contacts were not included.

atoms from the Phe34 phenyl ring. Hence, no stacking interactions between both π systems are observed. In the same way, the 4-methoxy group is not anchored in the electron rich region formed by Val115 and Ile7 carbonyl groups and by Tyr121 hydroxyl group (unlike the 4-amino group from Gangjee's inhibitors), but it is shifted toward the right side of the binding pocket. Also due to the inhibitor displacement toward the positive charged side of the pocket, the N_1—H bond from the 2-amino-4-methoxypyrimidine ring is interacting with Phe31 benzene ring instead of Glu30 carboxylate group.

As discussed above unlike the Gangjee's inhibitors, in compounds **16** and **18** the equivalent Pyr ring systems are more weakly bonded to the pocket than the C6- and N7-side-chains. In the case of compound **16**, it is even more weakly bonded than in compound **18**.

With regard to the C6- and N7-side-chains, the lack of a fused ring in compound **16** allows the rotation of these side-chains. Hence, they would be able to accommodate better into the binding pocket than in the more rigid **18** inhibitor. In fact, Figure 9 shows that the C6- and N7-rings of compound **16** are partially folded toward the lower and upper part of the pocket, respectively. In contrast, due to the lack of flexibility of the C6- and N7-side-chains of compound **18** they were somewhat bent from the plane of equivalent Pyr system due to interactions with different residues from the binding pocket, as shown before.

Figure 9b shows that the C6-side-chain ring is folded toward the bottom of the pocket where it is H-bonded to the positively charged residue Arg70, directly and also through a water molecule (not shown in the graph). The C6-side-chain of compound **16** is also interacting with the Phe31 carbonyl backbone through a (Phe31)C=O···H—C(C6-ring) H-bond, with the Gln35 side-chain through a (Gln35)C—H···π(C6-ring) H-bond and with Lys68 through a (Lys68)N$^+$—H···H—C(C6-ring) dihydrogen bond, among other minor interactions not shown in the graph. Moreover, N7-side-chain is folded toward the upper part of the pocket where it interacts strongly with Ile60 through several (Ile60)C—H···π(N7-ring) H-bonds.

Figure 10 shows the sum of the $\rho(r_b)$ values corresponding to the interactions of the Pyr system (blue bar) and C6-side-chain (red bar) obtained for the different inhibitors analyzed here. The sum of the $\rho(r_b)$ values for all the interactions of one part of the inhibitor (i.e., the Pyr ring system or the C6-side-chain) provides a measure of the anchoring strength of such moiety of the inhibitor to the binding pocket. Figure 10 clearly

shows that the classical inhibitors bind to the enzyme with similar strength through both parts of the molecule, the Pyr system and the C6-side-chain. Nonclassical inhibitors bind their Pyr portions with similar strength to that of the classical inhibitors. However, the anchoring through the C6-side-chain is much weaker in the nonclassical inhibitors than in the classical ones. As a result, the classical inhibitors such as **MTX**, **IN1**, and **IN2** are more strongly anchored in the binding pocket as evidenced by the greater total height of the stacked bars in Figure 10.

With respect to compounds **16** and **18**, the similar height of their stacked bars ($\rho(r_b) \approx 0.200$ au) indicates that both inhibitors are anchored with similar strength in the binding pocket. On average, these compounds are more weakly bonded to the binding pocket than the nonclassical inhibitors reported in ref 48 (most of the nonclassical Gangjee's inhibitors are bonded to the pocket with a total $\rho(r_b)$ value greater than 0.200 au; see Figure 10).

Analyzing the anchoring strength of each part of compounds **16** and **18** to the binding pocket, it can be observed that the equivalent Pyr systems are more weakly bonded to the pocket than the C6- and N7-side-chains. The equivalent Pyr system in compound **18** is slightly more strongly anchored than that of compound **16**. This is an important difference with the nonclassical Gangjee's inhibitors in which the Pyr ring systems are more tightly bonded to the pocket than the C6-side-chain (see Figure 10).

It also can be observed that the equivalent Pyr ring system is more weakly H-bonded to the active site in compounds **16** and **18** than in the nonclassical inhibitors (the Pyr ring systems from these inhibitors are anchored with a total $\rho(r_b)$ value greater than 0.150 au while, in compounds **16** and **18**, the density values at the anchor points are less than 0.100 au). In contrast, the C6- and N7-side-chain from compounds **16** and **18** are on average more strongly bonded to the binding pocket than the C6-side-chain from the nonclassical inhibitors (the C6-side-chains from Gangjee's inhibitors are bonded with a total $\rho(r_b)$ value lesser than 0.100 au except in **IN9**, while in compounds **16** and **18** they are greater than 0.100 au).

■ CONCLUSIONS

Accurate methods of computing the affinity of a small ligand interacting with the biological receptor are needed to spread the discovery of new leads. In our opinion, accurate calculations

2028

dx.doi.org/10.1021/ci400178h | J. Chem. Inf. Model. 2013, 53, 2018−2032

of enzyme–ligand binding affinities constitute an important and still unsolved problem. Nonetheless, significant progress is being made through a deeper understanding of the physical chemistry and the implementation of tractable approaches. In this regard, two important aspects have been taken into account in our study: on one hand, the design of reduced models that can be key to the validation and, second, the experimental corroboration, which remains indispensable for this purpose.

A molecular modeling study on 16 DHFR inhibitors was carried out. By combining MD simulations with ab initio and DFT calculations, a simple and generally applicable procedure to evaluate the binding energies of ligands interacting with the DHFR binding site has been reported here, providing a clear picture for the binding interactions of inhibitors from both structural and energetic points of view. Thus, our results provide interesting information which may be helpful in obtaining a deeper understanding of the molecular interactions between the ligands and the human DHFR enzyme.

The LIE method provides important information although somewhat limited. It is interesting to note that this type of calculations allows differentiating active compounds from nonactive ones.

In relation to the ab initio and DFT calculations, they show a better correlation when compared to those obtained by LIE. However, they provide limited information because their energies must be regarded as relative energies. Energetic calculations have been done using semiempirical geometric parameters (PM6), which might be affecting the correlation quality. However, significant correlations between binding energies obtained from PM6, ab initio, and DFT calculations with experimental IC_{50} values were obtained. Such correlations were experimentally corroborated synthesizing and testing two new inhibitors (compounds **16** and **18**). From our results, it is clear that the theoretical calculations reported here might predict the potential inhibitory effect of nonsynthesized compounds with an acceptable qualitative accuracy. Such information could be essential in order to know a priori the putative activity of new DHFR inhibitors.

It must be pointed out that, although the correlations obtained between the theoretical and experimental data are significant, they are not accurate enough to properly explain the different activities obtained for compounds possessing very similar IC_{50} values. Our results indicated that such differences might be explained only from a more exhaustive electronic analysis provided by QTAIM. However, we believe our results may be helpful in the structural identification and understanding of the minimum structural requirements for these molecules and may provide a guide in the design of new DHFR inhibitors.

ASSOCIATED CONTENT

ⓢ Supporting Information

Table 1S: Average ligand-surrounding energies obtained from MD simulations. Figure 1S: Histograms of interaction energies partitioned with respect to the hDHFR amino acids in complex with compounds **MTX**, **1**, **2**, **5**, **6**, and **8**. Figure 2S: Histograms of interaction energies for compounds **10**, **11**, **12**, and **13**. Figure 3S: Histograms of interaction energies for compounds **16** and **18**. Figure 4S: Molecular graphs of **IN3** interacting at the binding site. Figure 5S: Molecular graphs of **IN5** interacting at the binding site. Figure 6S: Top view of the Pyr ring in the binding pocket of complex hDHFR–**IN1** and complex hDHFR–**IN5**. This material is available free of charge via the Internet at http://pubs.acs.org.

AUTHOR INFORMATION

Corresponding Author
*Phone: (54) 266 4423789. E-mail: denriz@unsl.edu.ar.

Notes
The authors declare no competing financial interest.

REFERENCES

(1) Huennekens, F. M.; Duffy, T. H.; Vitols, K. S. Folic acid metabolism and its disruption by pharmacologic agents. *NCI Monogr.* **1987**, 1−8.

(2) Ingraham, H. A.; Dickey, L.; Goulian, M. DNA fragmentation and cytotoxicity from increased cellular deoxyuridylate. *Biochemistry* **1986**, 25, 3225−3230.

(3) Yoshioka, A.; Tanaka, S.; Hiraoka, O.; Koyama, Y.; Hirota, Y.; Ayusawa, D.; Seno, T.; Garrett, C.; Wataya, Y. Deoxyribonucleoside triphosphate imbalance. 5-Fluorodeoxyuridine-induced DNA double strand breaks in mouse FM3A cells and the mechanism of cell death. *J. Biol. Chem.* **1987**, 262, 8235−8241.

(4) Schnell, J. R.; Dyson, H. J.; Wright, P. E. Structure, dynamics, and catalytic function of dihydrofolate reductase. *Annu. Rev. Biophys. Biomol. Struct.* **2004**, 33, 119−140.

(5) Chan, D. C.; Fu, H.; Forsch, R. A.; Queener, S. F.; Rosowsky, A. Design, synthesis, and antifolate activity of new analogues of piritrexim and other diaminopyrimidine dihydrofolate reductase inhibitors with omega-carboxyalkoxy or omega-carboxy-1-alkynyl substitution in the side-chain. *J. Med. Chem.* **2005**, 48, 4420−4431.

(6) Gangjee, A.; Kurup, S.; Namjoshi, O. Dihydrofolate reductase as a target for chemotherapy in parasites. *Curr. Pharm. Des.* **2007**, 13, 609−639.

(7) Gangjee, A.; Jain, H. D.; Kurup, S. Recent advances in classical and non-classical antifolates as antitumor and antiopportunistic infection agents: part I. *Anticancer Agents Med. Chem.* **2007**, 7, 524−542.

(8) Gangjee, A.; Jain, H. D.; Kurup, S. Recent advances in classical and non-classical antifolates as antitumor and antiopportunistic infection agents: Part II. *Anticancer Agents Med. Chem.* **2008**, 8, 205−231.

(9) Champness, J. N.; Achari, A.; Ballantine, S. P.; Bryant, P. K.; Delves, C. J.; Stammers, D. K. The structure of Pneumocystis carinii dihydrofolate reductase to 1.9 Å resolution. *Structure* **1994**, 2, 915−924.

(10) Klon, A. E.; Heroux, A.; Ross, L. J.; Pathak, V.; Johnson, C. A.; Piper, J. R.; Borhani, D. W. Atomic structures of human dihydrofolate reductase complexed with NADPH and two lipophilic antifolates at 1.09 Å and 1.05 Å resolution. *J. Mol. Biol.* **2002**, 320, 677−693.

(11) Takimoto, C. H. Antifolates in clinical development. *Semin. Oncol.* **1997**, 24, S18−40−S18−51.

(12) Hamrell, M. R. Inhibition of dihydrofolate reductase and cell growth by antifolates in a methotrexate-resistant cell line. *Oncology* **1984**, 41, 343−348.

(13) Abel, E.; Lebwohl, M. Psoriasis. In *ACP Medicine*; Nabel, E. G., Ed.; BC Decker: Hamilton, ON, 2008; Chapter 3.

(14) Feagan, B. G.; Rochon, J.; Fedorak, R. N.; Irvine, E. J.; Wild, G.; Sutherland, L.; Steinhart, A. H.; Greenberg, G. R.; Gillies, R.; Hopkins, M.; Hanauer, S. B.; Mc Donald, J. W. D. Methotrexate for the treatment of Crohn's disease. The North American Crohn's Study Group Investigators. *N. Engl. J. Med.* **1995**, *332*, 292−297.

(15) Klippel, J. H.; Decker, J. L. Methotrexate in rheumatoid arthritis. *N. Engl. J. Med.* **1985**, *312*, 853−854.

(16) Weinblatt, M. E.; Coblyn, J. S.; Fox, D. A.; Fraser, P. A.; Holdsworth, D. E.; Glass, D. N.; Trentham, D. E. Efficacy of low-dose methotrexate in rheumatoid arthritis. *N. Engl. J. Med.* **1985**, *312*, 818−822.

(17) Wirth, D. Malaria: a 21st century solution for an ancient disease. *Nat. Med.* **1998**, *4*, 1360−1362.

(18) Klepser, M. E.; Klepser, T. B. Drug treatment of HIV-related opportunistic infections. *Drugs* **1997**, *53*, 40−73.

(19) Allegra, C. J.; Kovacs, J. A.; Drake, J. C.; Swan, J. C.; Chabner, B. A.; Masur, H. Activity of antifolates against Pneumocystis carinii dihydrofolate reductase and identification of a potent new agent. *J. Exp. Med.* **1987**, *165*, 926−931.

(20) Bartlett, M. S.; Shaw, M.; Navaran, P.; Smith, J. W.; Queener, S. F. Evaluation of potent inhibitors of dihydrofolate reductase in a culture model for growth of Pneumocystis carinii. *Antimicrob. Agents Chemother.* **1995**, *39*, 2436−2441.

(21) Fulton, B.; Wagstaff, A. J.; McTavish, D. Trimetrexate. A review of its pharmacodynamic and pharmacokinetic properties and therapeutic potential in the treatment of Pneumocystis carinii pneumonia. *Drugs* **1995**, *49*, 563−576.

(22) Hughes, D. T. Use of combinations of trimethoprim and sulphamethoxazole in the treatment of chest infections. *Med. J. Aust.* **1973**, *1* (Suppl), 58−61.

(23) Kasanen, A.; Anttila, M.; Elfving, R.; Kahela, P.; Saarimaa, H.; Sundquist, H.; Tikkanen, R.; Toivanen, P. Trimethoprim. Pharmacology, antimicrobial activity and clinical use in urinary tract infections. *Ann. Clin. Res.* **1978**, *10* (Suppl 22), 1−39.

(24) Salter, A. J. Trimethoprim-sulfamethoxazole in treatment of severe infections. *Rev. Infect. Dis.* **1982**, *4*, 338−350.

(25) Zhao, R.; Goldman, I. D. Resistance to antifolates. *Oncogene* **2003**, *22*, 7431−7457.

(26) Bleyer, W. A. The clinical pharmacology of methotrexate: new applications of an old drug. *Cancer* **1978**, *41*, 36−51.

(27) Izbicka, E.; Diaz, A.; Streeper, R.; Wick, M.; Campos, D.; Steffen, R.; Saunders, M. Distinct mechanistic activity profile of pralatrexate in comparison to other antifolates in in vitro and in vivo models of human cancers. *Cancer Chemother. Pharmacol.* **2009**, *64*, 993−999.

(28) Finland, M.; Kass, E. H. Trimethoprim-sulfamethoxazole. Summary and comments on the conference. *J. Infect. Dis.* **1973**, *128* (Suppl), 792−816.

(29) Saxena, A. K.; Saxena, M. Advances in chemotherapy of malaria. *Prog. Drug Res.* **1986**, *30*, 221−280.

(30) Lin, J. T.; Bertino, J. R. Update on trimetrexate, a folate antagonist with antineoplastic and antiprotozoal properties. *Cancer Invest.* **1991**, *9*, 159−172.

(31) Fraser, J. A.; Bartlett, J. Piritrexim (ILEX Oncology). *IDrugs* **1999**, *2*, 1183−1196.

(32) Goldman, I. D.; Chattopadhyay, S.; Zhao, R.; Moran, R. The antifolates: evolution, new agents in the clinic, and how targeting delivery via specific membrane transporters is driving the development of a next generation of folate analogs. *Curr. Opin. Investig. Drugs* **2010**, *11*, 1409−1423.

(33) Kollman, P. Free energy calculations: applications to chemical and biochemical phenomena. *Chem. Rev.* **1993**, *93*, 2395−2417.

(34) Carlson, H. A.; Jorgensen, W. L. An extended linear response method for determining free energies of hydration. *J. Phys. Chem.* **1995**, *99*, 10667−10673.

(35) Kollman, P. A.; Massova, I.; Reyes, C.; Kuhn, B.; Huo, S.; Chong, L.; Lee, M.; Lee, T.; Duan, Y.; Wang, W.; Donini, O.; Cieplak, P.; Srinivasan, J.; Case, D. A.; Cheatham, T. E., 3rd Calculating structures and free energies of complex molecules: combining molecular mechanics and continuum models. *Acc. Chem. Res.* **2000**, *33*, 889−897.

(36) Teramoto, R.; Fukunishi, H. Supervised consensus scoring for docking and virtual screening. *J. Chem. Inf. Model.* **2007**, *47*, 526−534.

(37) Bag, S.; Tawari, N. R.; Degani, M. S.; Queener, S. F. Design, synthesis, biological evaluation and computational investigation of novel inhibitors of dihydrofolate reductase of opportunistic pathogens. *Bioorg. Med. Chem.* **2010**, *18*, 3187−3197.

(38) *Glide*, version 5.0; Schrödinger, LLC: New York, NY, 2008.

(39) *Prime*, version 3.0; Schrödinger, LLC: New York, NY, 2008.

(40) Jacobson, M. P.; Pincus, D. L.; Rapp, C. S.; Day, T. J.; Honig, B.; Shaw, D. E.; Friesner, R. A. A hierarchical approach to all-atom protein loop prediction. *Proteins* **2004**, *55*, 351−367.

(41) Yu, Z.; Jacobson, M. P.; Friesner, R. A. What role do surfaces play in GB models? A new-generation of surface-generalized born model based on a novel gaussian surface for biomolecules. *J. Comput. Chem.* **2006**, *27*, 72−89.

(42) Kerrigan, J. E.; Abali, E. E.; Bertino, J. R. Recent Progress in Molecular Dynamics Simulations of Dihydrofolate Reductase. *Curr. Enzyme Inhib.* **2012**, *8*, 140−149.

(43) Oliveira, A. A.; Renno, M. N.; de Matos, C. A.; Bertuzzi, M. D.; Ramalho, T. C.; Fraga, C. A.; Franca, T. C. Molecular modeling studies of Yersinia pestis dihydrofolate reductase. *J. Biomol. Struct. Dyn.* **2011**, *29*, 351−367.

(44) Gokhale, V. M.; Kulkarni, V. M. Selectivity analysis of 5-(arylthio)-2,4-diaminoquinazolines as inhibitors of Candida albicans dihydrofolate reductase by molecular dynamics simulations. *J. Comput.-Aided Mol. Des.* **2000**, *14*, 495−506.

(45) Andujar, S.; Suvire, F.; Berenguer, I.; Cabedo, N.; Marin, P.; Moreno, L.; Dolores Ivorra, M.; Cortes, D.; Enriz, R. D. Tetrahydroisoquinolines acting as dopaminergic ligands. A molecular modeling study using MD simulations and QM calculations. *J. Mol. Model.* **2012**, *18*, 419−431.

(46) Andujar, S. A.; Tosso, R. D.; Suvire, F. D.; Angelina, E.; Peruchena, N.; Cabedo, N.; Cortes, D.; Enriz, R. D. Searching the "biologically relevant" conformation of dopamine: a computational approach. *J. Chem. Inf. Model.* **2012**, *52*, 99−112.

(47) Andujar, S. A.; de Angel, B. M.; Charris, J. E.; Israel, A.; Suarez-Roca, H.; Lopez, S. E.; Garrido, M. R.; Cabrera, E. V.; Visbal, G.; Rosales, C.; Suvire, F. D.; Enriz, R. D.; Angel-Guio, J. E. Synthesis, dopaminergic profile, and molecular dynamics calculations of N-aralkyl substituted 2-aminoindans. *Bioorg. Med. Chem.* **2008**, *16*, 3233−3244.

(48) Gangjee, A.; Zeng, Y.; Talreja, T.; McGuire, J. J.; Kisliuk, R. L.; Queener, S. F. Design and synthesis of classical and nonclassical 6-arylthio-2,4-diamino-5-ethylpyrrolo[2,3-d]pyrimidines as antifolates. *J. Med. Chem.* **2007**, *50*, 3046−3053.

(49) Ribeiro, A.; Horta, B.; de Alencastro, R. B. MKTOP: a program for automatic construction of molecular topologies. *J. Braz. Chem. Soc.* **2008**, *19*, 1433−1435.

(50) Berendsen, H. H.; van der Spoel, D.; van Drunen, R. GROMACS: a message-passing parallel molecular dynamics implementations. *Comput. Phys. Commun.* **1995**, *91*, 43−56.

(51) Lindahl, E.; Hess, B.; van der Spoel, D. GROMACS 3.0: a package for molecular simulations and trajectory analysis. *J. Mol. Model.* **2001**, *7*, 306−317.

(52) van Buuren, A.; Marrink, S.; Berendsen, H. H. A molecular dynamics study of the decane/water interface. *J. Phys. Chem.* **1993**, *36*, 9206−9212.

(53) Mark, A.; van Helden, S.; Smith, P.; Janssen, L.; van Gunsteren, W. Convergence properties of free energy calculations. A-cyclodextrin complexes as a case study. *J. Am. Chem. Soc.* **1994**, *116*, 6293−6302.

(54) Jorgensen, W.; Chandrasekhar, J.; Madura, J.; Impey, R.; Klein, M. Comparison of simple potential functions for simulating liquid water. *J. Chem. Phys.* **1983**, *79*, 926−935.

(55) van Buuren, A. R.; Berendsen, H. J. Molecular dynamics simulation of the stability of a 22-residue alpha-helix in water and 30% trifluoroethanol. *Biopolymers* **1993**, *33*, 1159−1166.

(56) Liu, H.; Muller-Plathe, F.; van Gunsteren, W. A Force Field for Liquid Dimethyl Sulfoxide and Physical Properties of Liquid Dimethyl Sulfoxide Calculated Using Molecular Dynamics Simulation. *J. Am. Chem. Soc.* **1995**, *117*, 4363−4366.

(57) Miyamoto, S.; Kollman, P. SETTLE-an analytical version of the SHAKE and RATTLE algorithm for rigid water models. *J. Comput. Chem.* **1992**, *13*, 952−962.

(58) Berendsen, H. J.; Postma, H.; van Gunsteren, W.; Hermans, W. Interaction models for water in relation to protein hydration. In *Intermolecular Forces*; Pullman, B., Ed.; Reidel: Dordrecht, The Netherlands, 1981; pp 331−342.

(59) Darden, T.; York, D.; Pedersen, L. Particle mesh Ewald - an N.log(n) method for Ewald sums in large systems. *J. Chem. Phys.* **1993**, *98*, 10089−10092.

(60) Bussi, G.; Donadio, D.; Parrinello, M. Canonical sampling through velocity rescaling. *J. Chem. Phys.* **2007**, *126* (014101), 1−7.

(61) Essmann, U.; Perera, L.; Berkowitz, M.; Darden, T.; Lee, H.; Pedersen, L. A smooth particle mesh Ewald method. *J. Chem. Phys.* **1995**, *103*, 8577−8593.

(62) Luty, B.; Tironi, I.; van Gunsteren, W. Lattice - sum methods for calculating electrostatic interactions in molecular simulations. *J. Chem. Phys.* **1995**, *103*, 3014−3021.

(63) Aqvist, J.; Medina, C.; Samuelsson, J. E. A new method for predicting binding affinity in computer-aided drug design. *Protein Eng.* **1994**, *7*, 385−391.

(64) Gutierrez-de-Teran, H.; Aqvist, J. Linear interaction energy: method and applications in drug design. *Methods Mol. Biol.* **2012**, *819*, 305−323.

(65) Hansson, T.; Marelius, J.; Aqvist, J. Ligand binding affinity prediction by linear interaction energy methods. *J. Comput.-Aided Mol. Des.* **1998**, *12*, 27−35.

(66) Marelius, J.; Graffner-Nordberg, M.; Hansson, T.; Hallberg, A.; Aqvist, J. Computation of affinity and selectivity: binding of 2,4-diaminopteridine and 2,4-diaminoquinazoline inhibitors to dihydrofolate reductases. *J. Comput.-Aided Mol. Des.* **1998**, *12*, 119−131.

(67) Oefner, C.; D'Arcy, A.; Winkler, F. K. Crystal structure of human dihydrofolate reductase complexed with folate. *Eur. J. Biochem.* **1988**, *174*, 377−385.

(68) Davies, J. F., 2nd; Delcamp, T. J.; Prendergast, N. J.; Ashford, V. A.; Freisheim, J. H.; Kraut, J. Crystal structures of recombinant human dihydrofolate reductase complexed with folate and 5-deazafolate. *Biochemistry* **1990**, *29*, 9467−9479.

(69) Case, D. A.; Darden, T. A.; Cheatham, T. E., III; Simmerling, C. L.; Wang, J.; Duke, R. E.; Luo, R.; Walker, R. C.; Zhang, W.; Merz, K. M.; Roberts, B.; Hayik, S.; Roitberg, A.; Seabra, G.; Swails, J.; Goetz, A. W.; Kolossváry, I.; Wong, K. F.; Paesani, F.; Vanicek, J.; Wolf, R. M.; Liu, J.; Wu, X.; Brozell, S. R.; Steinbrecher, T.; Gohlke, H.; Cai, Q.; Ye, X.; Wang, J.; Hsieh, M.-J.; Cui, G.; Roe, D. R.; Mathews, D. H.; Seetin, M. G.; Salomon-Ferrer, R.; Sagui, C.; Babin, V.; Luchko, T.; Gusarov, S.; Kovalenko, A.; Kollman, P. A. *AMBER12*; University of California, San Francisco, CA, 2012.

(70) Hou, T.; Li, N.; Li, Y.; Wang, W. Characterization of domain-peptide interaction interface: prediction of SH3 domain-mediated protein-protein interaction network in yeast by generic structure-based models. *J. Proteome Res.* **2012**, *11*, 2982−2995.

(71) Gohlke, H.; Kiel, C.; Case, D. A. Insights into protein-protein binding by binding free energy calculation and free energy decomposition for the Ras-Raf and Ras-RalGDS complexes. *J. Mol. Biol.* **2003**, *330*, 891−913.

(72) Hou, T.; Zhang, W.; Case, D. A.; Wang, W. Characterization of domain-peptide interaction interface: a case study on the amphiphysin-1 SH3 domain. *J. Mol. Biol.* **2008**, *376*, 1201−1214.

(73) Hou, T.; Xu, Z.; Zhang, W.; McLaughlin, W. A.; Case, D. A.; Xu, Y.; Wang, W. Characterization of domain-peptide interaction interface: a generic structure-based model to decipher the binding specificity of SH3 domains. *Mol. Cell Proteom.* **2009**, *8*, 639−649.

(74) Hou, T.; Li, Y.; Wang, W. Prediction of peptides binding to the PKA RIIalpha subunit using a hierarchical strategy. *Bioinformatics* **2011**, *27*, 1814−1821.

(75) Stewart, J. J. P. Optimization of parameters for semiempirical methods V: modification of NDDO approximations and application to 70 elements. *J. Mol. Model.* **2007**, *13*, 1173−1213.

(76) Stewart, J. J. P. *MOPAC2009*; Stewart Computational Chemistry: Colorado Springs, CO, 2008.

(77) Frisch, M. J.; Trucks, G. W.; Schlegel, H. B.; Scuseria, G. E.; Robb, M. A.; Cheeseman, J. R.; Montgomery, J. A., Jr.; Vreven, T.; Kudin, K. N.; Burant, J. C.; Millam, J. M.; Iyengar, S. S.; Tomasi, J.; Barone, V.; Mennucci, B.; Cossi, M.; Scalmani, G.; Rega, N.; Petersson, G. A.; Nakatsuji, H.; Hada, M.; Ehara, M.; Toyota, K.; Fukuda, R.; Hasegawa, J.; Ishida, M.; Nakajima, T.; Honda, Y.; Kitao, O.; Nakai, H.; Klene, M.; Li, X.; Knox, J. E.; Hratchian, H. P.; Cross, J. B.; Adamo, C.; Jaramillo, J.; Gomperts, R.; Stratmann, R. E.; Yazyev, O.; Austin, A. J.; Cammi, R.; Pomelli, C.; Ochterski, J. W.; Ayala, P. Y.; Morokuma, K.; Voth, G. A.; Salvador, P.; Dannenberg, J. J.; Zakrzewski, V. G.; Dapprich, S.; Daniels, A. D.; Strain, M. C.; Farkas, O.; Malick, D. K.; Rabuck, A. D.; Raghavachari, K.; Foresman, J. B.; Ortiz, J. V.; Cui, Q.; Baboul, A. G.; Clifford, S.; Cioslowski, J.; Stefanov, B. B.; Liu, G.; Liashenko, A.; Piskorz, P.; Komaromi, I.; Martin, R. L.; Fox, D. J.; Keith, T.; Al-Laham, M. A.; Peng, C. Y.; Nanayakkara, A.; Challacombe, M.; Gill, P. M. W.; Johnson, B.; Chen, W.; Wong, M. W.; Gonzalez, C.; Pople, J. A. *Gaussian 03*, revision B.05; Gaussian Inc.: Pittsburgh, PA, 2003.

(78) Keith, T. *AIMA11*, version 12.11.09; Gristmill Software: Overland Park, KS, 2012.

(79) Castillo, N.; Boyd, R. J. A theoretical study of the fluorine valence shell in methyl fluoride. *Chem. Phys. Lett.* **2005**, *403*, 47−54.

(80) Jablonski, M.; Palusiak, M. Basis set and method dependence in quantum theory of atoms in molecules calculations for covalent bonds. *J. Phys. Chem. A* **2010**, *114*, 12498−12505.

(81) Matta, C. F. How dependent are molecular and atomic properties on the electronic structure method? Comparison of Hartree-Fock, DFT, and MP2 on a biologically relevant set of molecules. *J. Comput. Chem.* **2010**, *31*, 1297−1311.

(82) Pettersen, E. F.; Goddard, T. D.; Huang, C. C.; Couch, G. S.; Greenblatt, D. M.; Meng, E. C.; Ferrin, T. E. UCSF Chimera–a visualization system for exploratory research and analysis. *J. Comput. Chem.* **2004**, *25*, 1605−1612.

(83) Florián, J.; Hrouda, V.; Hobza, P. Proton transfer in the Adenine-Thymine base pair. *J. Am. Chem. Soc.* **1994**, *116*, 1457−1460.

(84) Florián, J.; Leszczynski, J. Spontaneous DNA mutations induced by proton transfer in the Guanine-Cytosine base pairs: an energetic perspective. *J. Am. Chem. Soc.* **1996**, *118*, 3010−3017.

(85) Alemán, C. The keto-amino/enol tautomerism of cytosine in aqueous solution. A theoretical study using combined discrete/self-consistent reaction field models. *Chem. Phys.* **2000**, *253*, 13−19.

(86) Gready, J. E. Dihydrofolate reductase: binding of substrates and inhibitors and catalytic mechanism. *Adv. Pharmacol. Chemother.* **1980**, *17*, 37−102.

(87) Blakley, R. L. Eukaryotic dihydrofolate reductase. *Adv. Enzymol. Relat. Areas Mol. Biol.* **1995**, *70*, 23−102.

(88) Costi, M. P.; Ferrari, S. Update on antifolate drugs targets. *Curr. Drug Targets* **2001**, *2*, 135−166.

(89) Schweitzer, B. I.; Dicker, A. P.; Bertino, J. R. Dihydrofolate reductase as a therapeutic target. *Faseb J.* **1990**, *4*, 2441−2452.

(90) Mathews, C. K.; Scrimgeour, K. G.; Huennekens, F. M. Dihydrofolate reductase. *Methods Enzymol.* **1963**, *6*, 364−368.

(91) Hillcoat, B. L.; Nixon, P. F.; Blakley, R. L. Effect of substrate decomposition on the spectrophotometric assay of dihydrofolate reductase. *Anal. Biochem.* **1967**, *21*, 178−189.

(92) Schweitzer, B. I.; Srimatkandada, S.; Gritsman, H.; Sheridan, R.; Venkataraghavan, R.; Bertino, J. R. Probing the role of two hydrophobic active site residues in the human dihydrofolate reductase by site-directed mutagenesis. *J. Biol. Chem.* **1989**, *264*, 20786−20795.

(93) Piper, J. R.; Montgomery, J. A.; Sirotnak, F. M.; Chello, P. L. Syntheses of alpha- and gamma-substituted amides, peptides, and esters of methotrexate and their evaluation as inhibitors of folate metabolism. *J. Med. Chem.* **1982**, *25*, 182−187.

(94) Bader, R. F. W. *Atoms in Molecules: A Quantum Theory*; Oxford University Press: Oxford, U.K., 1994.

(95) Matta, C. F.; Boyd, R. J. *The Quantum Theory of Atoms in Molecules: From Solid State to DNA and Drug Design*; Wiley-VCH: Weinheim, Germany, 2007.

(96) Koch, U.; Popelier, P. L. A. Characterization of C−H···O Hydrogen Bonds on the Basis of the Charge Density. *J. Phys. Chem.* **1995**, *99*, 9747−9754.

(97) Matta, C. F.; Castillo, N.; Boyd, R. J. Extended Weak Bonding Interactions in DNA: π-Stacking (Base−Base), Base−Backbone, and Backbone−Backbone Interactions. *J. Phys. Chem. B* **2005**, *110*, 563−578.

(98) Mosquera, R. A.; Moa, M. J. G.; Estévez, L.; Mandado, M.; Graña, A. M. An Electron Density-Based Approach to the Origin of Stacking Interactions. In *Quantum Biochemistry*; Matta, C. F., Ed.; WILEY-VCH Verlag GmbH & Co. KGaA: Weinheim, Germany, 2010; pp 365−387.